J Electroceram (2011) 26:56–62
DOI 10.1007/s10832-010-9627-2

# Measurement of electrical conductivity of $La_{0.2}Sr_{0.8}Cr_{0.2}Fe_{0.8}O_{3-\delta}$ using gas-tight electrochemical cells

**Jiho Yoo · Sangdo Kim · Hokyung Choi · Youngjoon Rhim · Jeonghwan Lim · Sihyun Lee · Allan J. Jacobson**

Received: 26 May 2010 / Accepted: 23 December 2010 / Published online: 11 January 2011


**Abstract** The oxygen partial pressure ($pO_2$) dependence of the electrical conductivity of $La_{0.2}Sr_{0.8}Cr_{0.2}Fe_{0.8}O_{3-\delta}$ (LSCrF) was obtained at $T$=750–1060°C and $pO_2$= $10^{-18}$–0.5 atm. The slope of the plot of log σ vs. log $pO_2$ is ~1/5 in the p–type region, $pO_2=10^{-5}$–$10^{-1}$ atm. The p-n transition $pO_2$ increases with increasing temperature. The activation energy for ionic conduction was estimated to be 0.86 eV from an Arrhenius plot of the minimum conductivity vs. reciprocal temperature. At temperatures below 942°C, a plateau in the conductivity isotherm suggests the presence of a two-phase region. Most likely, phase separation occurs to form a mixture of a perovskite phase and an oxygen vacancy ordered phase related to brownmillerite.

**Keyword** $La_{0.2}Sr_{0.8}Cr_{0.2}Fe_{0.8}O_{3-\delta}$ · Perovskite · Electrical conductivity · SOFC

## 1 Introduction

Oxides with the perovskite structure have been widely studied because they are candidate materials for practical applications. Depending on the specific properties of the oxide, they can be utilized as electrodes or interconnect materials in solid oxide fuel cells (SOFCs), as permselective gas membranes, as electrochemical sensors, and in membrane reactors for syngas production [1–4]. Even though each application has its own requirements, in general the perovskite oxides should have both high conductivity and structural stability.

Many groups have investigated aspects of the solid-state chemistry of $La_{1-x}Sr_xFeO_{3-\delta}$, ($x$=0.1~0.9), including the kinetics of oxygen permeation, defect structure, and the $pO_2$ dependence of conductivity and oxygen non-stoichiometry [5–12]. As the ferrites are mixed ionic and electronic conductors (MIECs) with high oxygen permeability and better stability than the $La_{1-x}Sr_xCoO_{3-\delta}$ series, they can be used for oxygen separation membranes. They may not, however, have adequate stability to be used in the reducing environment present in syngas processes.

The system $La_{1-x}Sr_xCrO_{3-\delta}$ combines relatively high electronic conductivity with enhanced stability in reducing condition, [13–18] and thus has been studied as an interconnect material in SOFCs. At elevated temperatures the electrical conductivity of Sr- and Ca-doped $LaCrO_{3-\delta}$ was found to be ≈ 10–100 S/cm and thermally activated with activation energies of 0.1–0.2 eV. The small activation energy is indicative of small polaron hopping transport [19–21]. In addition, conductivities are not influenced by the $pO_2$ change in oxidizing region, [20, 21] demonstrating good stability against reduction. The electrical conductivity increases with increasing the amount of Sr dopant in the range, $x$=0–0.3 [13]. When the dopant concentration is further increased ($x$=0.4 and 0.5), the anionic charge is compensated dominantly by the formation of oxygen vacancies. The inclusion of chromium ions onto the B-sites of the perovskite lattice could

J. Yoo (✉) · S. Kim · H. Choi · Y. Rhim · J. Lim · S. Lee
Climate Change Technology Division,
Korea Institute of Energy Research,
102 Gajeong-ro, Yuseong-gu,
Daejeon 305-343, Korea
e-mail: jyoo@kier.re.kr

A. J. Jacobson
Department of Chemistry, University of Houston,
4800 Calhoun Rd,
Houston, TX 77004, USA

enhance the stability. However, poor sinterability caused by the volatilization of chromium metals at high temperature, must be overcome to prepare dense materials [22].

The redox stability of the transition metal occupying the B-site of the perovskite lattice generally reflects the chemical stability of the corresponding perovskite oxide. The relative stability of the first row transition metal systems is in the order $Cr^{3+} > Fe^{3+} > Mn^{3+} > Co^{3+}$, and is opposite to the general trends in the ionic conductivity and oxygen permeability [23]. As a consequence many combinations of B site cations have been investigated in order to find the best compromise in properties for high temperature, low $pO_2$ applications [24–27]. The composition $La_{0.2}Sr_{0.8}Cr_{0.2}Fe_{0.8}O_{3-\delta}$ (LSCrF) is one example of a system that has adequate stability and conductivity for syngas generation [28]. Only limited information is, however, available on the $pO_2$ dependence of its conductivity.

Using sealed electrochemical cells, the electrical conductivity was measured on LSCrF in the temperature range, 750–1060°C and in the oxygen partial pressure ($pO_2$) range, $10^{-18}$–0.5 atm. The experimental set-up enabled us to accurately control $pO_2$ and thereby the sample non-stoichiometry. In the present work the oxygen partial pressure dependence of conductivities are described. In certain ranges of $pO_2$ and T, equilibration is difficult to achieve and consequently the issues associated with achieving equilibrium are discussed in some detail.

## 2 Experimental

LSCrF powder was purchased from Praxair specialty ceramics (lot number: 03-P3102DM). A combustion spray pyrolysis process was used to synthesize the powder, which had 99.9% chemical purity. The powder was pressed to form a 2.5 cm diameter pellet with 2.5–5.0 mm thickness. The pellet was cold isostatically pressed at 40,000 psi. The sample was then sintered at 1150°C for 8 h with heating and cooling rates of 1°C / min. Finally rectangular sample bars (~18 mm×~2.2 mm×~2.5 mm) were cut for the conductivity experiments. The sample was compositionally homogeneous and single phase with a density of ≈93% of the theoretical density [29].

The details of the electrical conductivity measurements can be found elsewhere [30–32, 35]. As shown in Fig. 1, the wall of the cell was built by stacking alumina rings (OD=12 mm, thickness = 1.5 mm, and height = 3~10 mm) and Pyrex glass rings (OD=12 mm, thickness = 1.5 mm, and height = 0.5–1 mm) one by one. Both the top and the bottom of the cell were closed with YSZ discs. The top YSZ disc was used as a sensor monitoring $pO_2$ inside the cell with air as the reference gas on the outside;

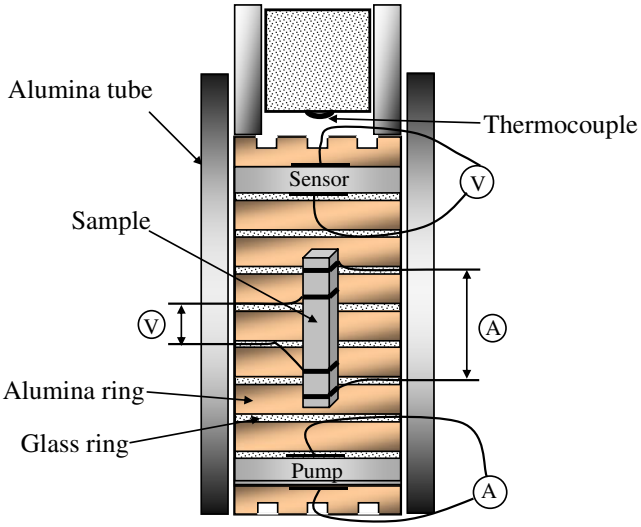


**Fig. 1** A schematic of the electrochemical cell

the bottom YSZ was used as a pump to control the oxygen fluxes into the cell and thereby the $pO_2$. As YSZ is a pure oxide ion conductor, it can be used to remove or supply oxygen quantitatively down to very low $pO_2$s. Four Pt wires were linked to the rectangular sample bar that was placed in the middle of the cell. The Pt wires inside the cell were brought out through the glass rings. The cell became gas-tight when the temperature was raised above 821°C and the glass rings softened. The EMF of the sensor was measured by using Keithley 2000-20 multimeter. A Keithley 2400 SourceMeter was used as the pump current source. The experiments were controlled by LabView software through a GPIB communicator. An AC four-point probe technique was used to monitor the conductivity of the sample with a lock-in amplifier (Stanford Research Systems: Model SR 830 DSP).

The electrical conductivity of LSCrF was determined at $750 \leq T \leq 1060°C$ and $10^{-18} \leq pO_2 \leq 0.5$ atm. The measurements were usually made on increasing $pO_2$ (from low to high $pO_2$). The cell was initially pumped out down to $pO_2 \approx 10^{-18}$ atm. The conductivities were monitored as a function of $pO_2$ stepwise. After pumping a known amount of oxygen into the cell, the conductivity was determined when the new equilibrium state was reached. A variation in the conductivity by less than 0.1% per a minute was used as the criterion for equilibrium. The procedure was repeated up to the $pO_2 \approx 0.5$ atm. The measurements were also made on decreasing $pO_2$ (from high to low $pO_2$) to confirm the reproducibility of the measurements, and using other cells.

Solid-state coulometric titrations were performed in the similar electrochemical cell [31, 32, 35]. The configuration is much simpler, since extra sealing for conductivity leads are not required.

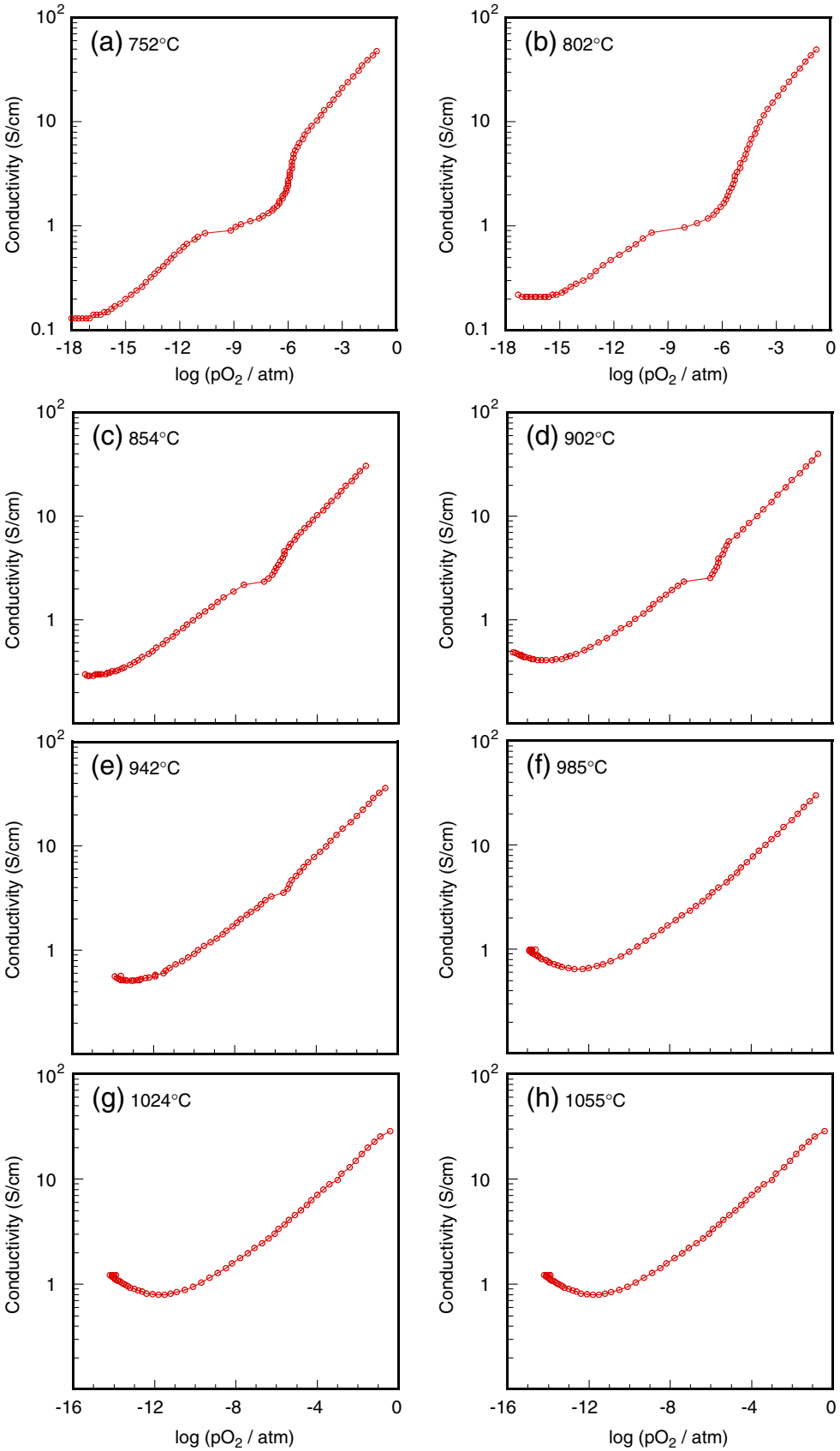


**Fig. 2** $pO_2$ dependence of electrical conductivities at 752, 802, 854, 902, 942, 985, 1024, and 1055°C

## 3 Results

The $pO_2$ dependence of the electrical conductivity at 752, 802, 854, 902, 942, 985, 1024, and 1055°C was determined with increasing oxygen partial pressure ($pO_2$) after the cell had been initially pumped out (Fig. 2). When the temperature increases, the conductivity decreases in the higher $pO_2$ region ($pO_2 > 10^{-5}$ atm) due to an increase in the oxygen vacancy concentration, thus reducing the electron hole concentration (Fig. 3). The profile of the conductivity is temperature dependent. At $T \leq 942$°C, a plateau and a steep slope occur in the middle $pO_2$ region ($10^{-10}$–$10^{-5}$ atm), but at the higher temperatures they disappear. At $752 \leq T \leq 942$°C, the general trends of the $pO_2$ dependence are very similar to one another, but the size of the discontinuity becomes larger systematically on decreasing the temperature. The p to n transition $pO_2$ (where the conductivity minimum is positioned) increases with increasing temperature.

The conductivity measurements were repeated with two different cells to confirm the reproducibility. Two conductivity isotherms obtained at 850°C on increasing $pO_2$ (from low to high $pO_2$) are compared in Fig. 4. In the plot, #2 was measured with a larger size of the $pO_2$ composition step than #1. The conductivity isotherms are generally reproducible except in the middle $pO_2$ region where a plateau and a steep slope appear. The larger $pO_2$ step (#2) leads to much wider discontinuity, indicating non-equilibrium. Similar trend is expected for the isotherms observed at the lower temperatures ($T \leq 940$°C). The profile of the isotherms at $T \leq 940$°C also varies depending on the direction of the $pO_2$ change. In Fig. 5, we show conductivity data at 900°C and 940°C, measured in the opposite direction, namely from high to low $pO_2$. This direction shows no plateau region at the intermediate $pO_2$ values but only a change in the slope. The data at both high and low partial pressures agree with the measurements made in the reverse direction (note that a set of data in Fig. 5 are offset for clarity). Apparently the phase separation is faster from the high-pressure side but whether this is an intrinsic phenomenon or related to mass transfer effects is not known.

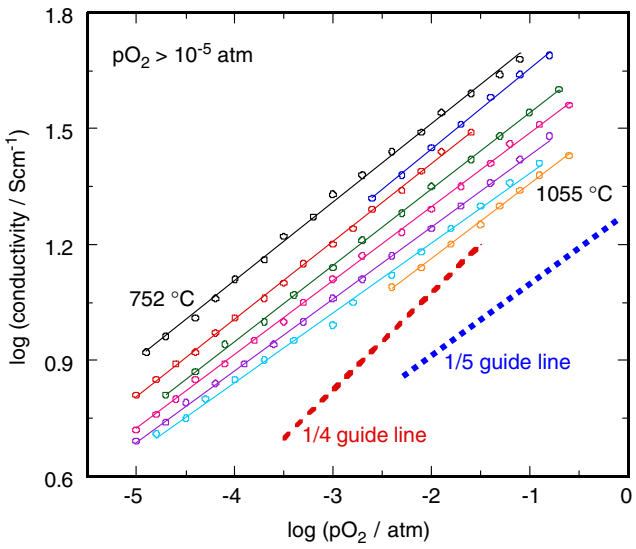


**Fig. 3** $pO_2$ dependence of electrical conductivities at $pO_2 \geq 10^{-5}$ atm

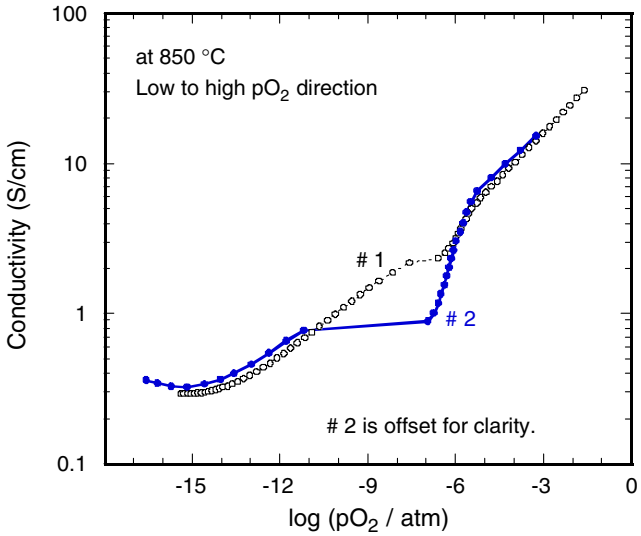


**Fig. 4** Two conductivity isotherms of $La_{0.2}Sr_{0.8}Cr_{0.2}Fe_{0.8}O_{3-\delta}$ at 850°C. # 2 is obtained with a larger size of the $pO_2$ composition step than # 1

At ≥980°C, where no plateau is observed, reproducibility is achieved over the whole $pO_2$ range, irrespective of the direction of the $pO_2$ change (either "low to high $pO_2$" or "high to low $pO_2$") [31, 32, 35].

## 4 Discussion

The plateau region observed in the $pO_2$ variation of the conductivity suggests that a two-phase region exists in the temperature range below 942°C (Fig. 2). At high vacancy concentrations and lower temperatures perovskite oxides often phase separate and form vacancy ordered phases to reduce coulombic repulsion among defects [30–35]. The kinetics of phase separations between ordered and disordered systems are known to be slow in perovskite oxides as discussed for $SrFe_{0.2}Co_{0.8}O_{3-x}$ [36]. The associated rearrangement of metallic cations seems to be responsible for the slower equilibration at the intermediate $pO_2$ values. Therefore, the time to reach equilibrium varies significantly depending on the $pO_2$ for the conductivity measurements [31, 35]. The general shape of the data at $T \leq 940$°C (Figs. 2, 4, and 5) suggests that equilibrium is not achieved in the

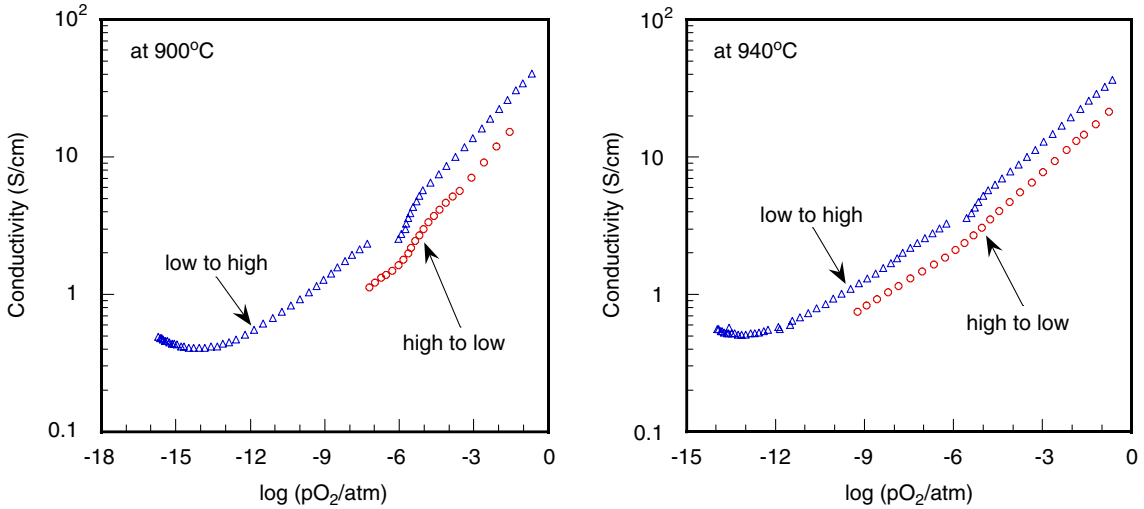


**Fig. 5** Comparison of conductivity isotherms according to the $pO_2$ direction: "high to low $pO_2$" run and "low to high $pO_2$" run. For clarity, "high to low $pO_2$" runs are positioned downward

middle $pO_2$ region, but in both the higher ($pO_2 > 10^{-5}$ atm) and the lower ($pO_2 < 10^{-10}$ atm) area.

Specifically, if a well-defined two-phase region exists then the conductivity should change discontinuously at the $pO_2$ value at which the two phases are in equilibrium. The magnitude of the discontinuity will depend on the difference in total conductivity between the two phases. The ionic conductivity is directly affected by the vacancy ordering and the electronic conductivity depends on the consequent changes in the electronic structure. The total effect on the conductivity is not easy to predict but general, we might expect the difference to be small since the two phases have similar composition [31, 35]. We note that the change is reported to be small in $SrFeO_{3-\delta}$. [37]. The observed behavior can be interpreted as follows. At a given temperature, on increasing $pO_2$, the conductivity increases from the minimum, through a p-type region, until the plateau is reached. The conductivity then remains constant until a large enough excess oxygen pressure (over-potential) is applied to drive the phase transition. As the phase transition occurs, the conductivity increases until the high-pressure equilibrium line is reached. The size of the plateau region decreases with increasing temperature both because the rate of the phase separation increases and also because the width of the two phase region decreases. By 985°C, the plateau region is no longer apparent. The $pO_2$ dependence of oxygen non-stoichiometry ($\delta$) has been measured. The experimental raw data at 800°C is given in the form of a plot of the relative $\delta$ vs. log $pO_2$ and compared with the conductivity result (Fig. 6). The absence of any change in $\delta$ at the $pO_2$ range corresponding to the plateau in the conductivity data is also consistent with the above interpretation. The changes in the stoichiometry as a function of T and $pO_2$ will be discussed in a future publication.

The slope of the isotherms is dependent on $pO_2$, and is ~1/5 almost irrespective of T in the p-type region, $pO_2 \geq 10^{-5}$ atm (Fig. 3). For non-interacting and dilute defects, $\sigma$ is proportional to $(pO_2)^{1/4}$, assuming constant mobility [38, 39]. Since 80% of the A site is occupied with Sr, high oxygen deficiency is observed at elevated T and hence defect interactions and association are expected, leading to lower values of the exponent. In the $pO_2$ range between the plateau and the minimum value of $\sigma$ in the isotherms, the electrical conductivity values are nearly independent of temperature (Fig. 7). For example, at $pO_2 = 10^{-10}$ atm the conductivity varies from 0.8 to 1.1 S/cm, regardless of the temperatures. The total conductivity ($\sigma$) is approximately the sum of the electron hole conductivity ($\sigma_h$) and the ionic conductivity ($\sigma_i$) in this region. Since the values of $\sigma_h$ and

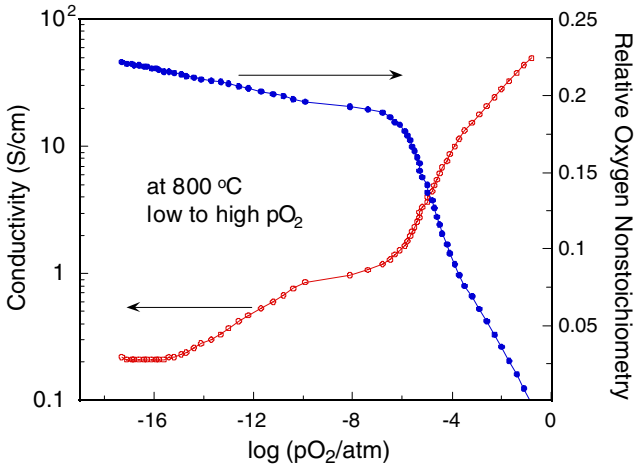


**Fig. 6** For $La_{0.2}Sr_{0.8}Cr_{0.2}Fe_{0.8}O_{3-\delta}$, the conductivity result is compared with the relative oxygen non-stoichiometry ($\delta$) isotherm at 800°C. Solid lines are drawn to guide the eye

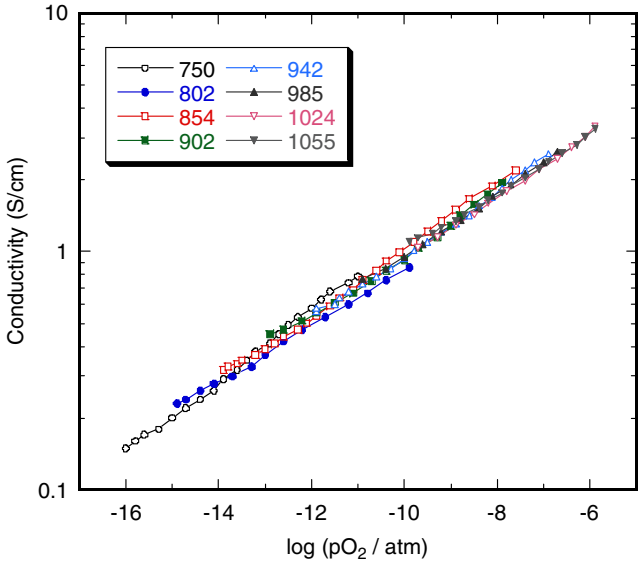


**Fig. 7** $pO_2$ dependence of electrical conductivities of $La_{0.2}Sr_{0.8}Cr_{0.2}Fe_{0.8}O_{3-\delta}$ in the $pO_2$ range between the plateau and the conductivity minima

$\sigma_i$ are comparable in this $pO_2$ range, a $\sigma \propto (pO_2)^{1/4}$ dependence is not expected. The weak temperature dependence arises because of the opposite temperature dependences of $\sigma_h$ and $\sigma_i$. Thus, the decrease in $\sigma_h$ at higher T is compensated by a higher $\sigma_i$.

The conductivity isotherms in the vicinity of the p-n transition $pO_2$ are shown in Fig. 8. Oxygen partial pressure at the conductivity minimum ($\sigma_{min}$) increases with increasing temperature. The p-n transitions of LSCrF occur at $pO_2$ (atm)=$2.36\times10^{-18}$–$6.80\times10^{-12}$ at $T$=752–1055°C (Table 1). At the $pO_2$ values corresponding to the minimum conductivities ($\sigma_{min}$) (Table 1), the ionic

**Table 1** Oxygen partial pressure ($pO_2$) and the conductivity at the p-n transition point

| T (°C) | p-n transition $pO_2$ (atm) | $\sigma_{min}$ (S/cm) |
|---|---|---|
| 752 | $2.36\times10^{-18}$ | 0.13 |
| 802 | $3.65\times10^{-17}$ | 0.21 |
| 854 | $6.99\times10^{-16}$ | 0.29 |
| 902 | $8.67\times10^{-15}$ | 0.41 |
| 942 | $7.41\times10^{-14}$ | 0.51 |
| 985 | $2.20\times10^{-13}$ | 0.65 |
| 1024 | $1.67\times10^{-12}$ | 0.80 |
| 1055 | $6.80\times10^{-12}$ | 1.00 |

transference numbers approach unity and the oxygen vacancy concentrations are independent of the temperature [40, 41]. Thus, activation energy ($E_a$) is mainly due to the ionic mobility term in the conductivity [38]. Assuming that $\sigma_{min}T = A \cdot \exp(-E_a/RT)$, then a plot of log ($\sigma_{min}T$) vs.1000/T, (Fig. 9) gives an activation energy of 0.86 eV for ionic conduction.

## 5 Conclusion

Electrical conductivity measurements have been performed on $La_{0.2}Sr_{0.8}Cr_{0.2}Fe_{0.8}O_{3-\delta}$ (LSCrF) in the temperature range, 750–1060°C and in the $pO_2$ range, $10^{-18}$–0.5 atm. In the $pO_2$ range from $10^{-5}$–$10^{-1}$ atm the conductivity is proportional to $(pO_2)^{0.2}$, somewhat lower than the 0.25 dependence expected for an ideal system of doubly ionized oxygen vacancies. At intermediate oxygen partial pressures, the conductivity shows only weak temperature dependence.

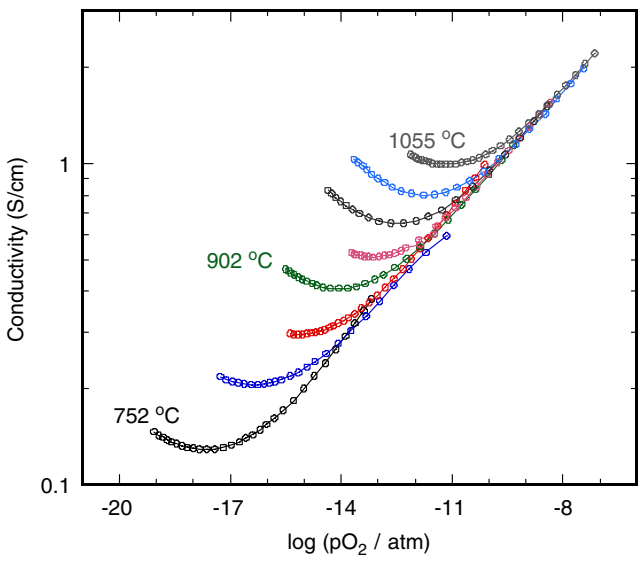


**Fig. 8** Temperature dependence of p-n transition behavior

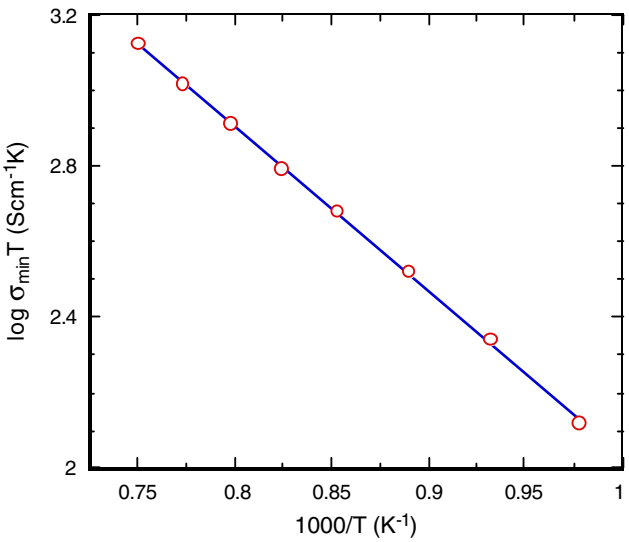


**Fig. 9** Arrhenius plot of $\sigma_i$ at the $pO_2$ where the p-n transition occurs

At low $pO_2$, a p-n transition is observed. From the temperature dependence of the $pO_2$ at which the minimum conductivity is observed, the activation energy for ionic conduction was estimated to be 0.86 eV. At temperatures below 940°C, a plateau in the conductivity isotherms indicates the presence of a two-phase region most probably corresponding to a mixture of perovskite and oxygen vacancy ordered phases.

## References


1. K. Vidala, L.M.R. Martínezb, L.O.S. Martinc, A.M. Amesti, M.L. Nóa, T. Rojoa, A. Laresgoiti, M.I. Arriortua, J. Power Sources **192**, 175 (2009)
2. P. Zenga, Z. Chena, W. Zhoua, H. Gua, Z. Shao, S. Liu, J. Membrane Sci. **291**, 148 (2007)
3. H. Luoa, Y. Weia, H. Jiangb, W. Yuana, Y. Lva, J. Carob, H. Wang, J. Membrane Sci. **350**, 154 (2010)
4. J. Zosel, D. Franke, K. Ahlborn, F. Gerlach, V. Vashook, U. Guth, Solid State Ionics **179**, 1628 (2008)
5. I. Waernhus, N. Sakai, H. Yokokawa, T. Grande, M.A. Einarsrud, K. Wiik, Solid State Ionics **175**, 69 (2004)
6. J. Mizusaki, M. Yoshihiro, S. Yamauchi, K. Fueki, J. Solid State Chem. **58**, 257 (1985)
7. M.V. Patrakeev, I.A. Leonidov, V.L. Kozhevnikov, K.R. Poeppelmeier, J. Solid State Chem. **178**(3), 921 (2005)
8. M.C. Kim, S.J. Park, Solid State Ionics **40/41**, 239 (1990)
9. M.V. Patrakeev, J.A. Bahteeva, E.B. Mitberg, I.A. Leonidov, V.L. Kozhevnikov, K.R. Poeppelmeier, J. Solid State Chem. **172**(1), 219 (2003)
10. J.E. ten Elshof, H.J.M. Bouwmeester, H. Verweij, Solid State Ionics **81**, 97 (1995)
11. S.E. Dann, D.B. Currie, M.T. Weller, M.F. Thomas, A.D. AL-Rawwas, J. Solid States Chem. **109**, 134 (1994)
12. J. Mizusaki, M. Yoshihiro, S. Yamauchi, K. Fueki, J. Solid State Chem. **67**, 1 (1987)
13. X. Liu, W. Su, Z. Lu, J. Liu, L. Pei, W. Liu, L. He, J. Alloys Compds **305**, 21 (2000)
14. H.U. Anderson, Solid State Ionics **52**, 33 (1992)
15. S. Miyoshi, S. Onuma, A. Kaimai, H. Matsumoto, K. Yashiro, T. Kawada, J. Mizusaki, H. Yokokawa, J. Solid State Chem. **177**, 4112 (2004)
16. L. Groupp, H.U. Anderson, J. Am. Ceram. Soc. **59**, 449 (1976)
17. S. Onuma, K. Yashiro, S. Miyoshi, A. Kaimai, H. Matsumoto, Y. Nigara, T. Kawada, J. Mizusaki, K. Kawamura, N. Sakai, H. Yokokawa, Solid State Ionics **174**, 287 (2004)
18. A.A. Yaremchenko, V.V. Kharton, A.L. Shaula, M.V. Patrakeev, F.M.B. Marques, J. Eur. Ceram. Soc. **25**, 2603 (2005)
19. D.P. Karim, A.T. Aldred, Phys. Rev. B **20**(6), 2255 (1979)
20. I. Yasuda, T. Hikita, J. Electrochem. Soc. **140**(6), 1699 (1993)
21. I. Yasuda, M. Hishinuma, Solid State Ionics **80**, 141 (1995)
22. H. Yokokawa, N. Sakai, T. Kawada, M. Dokiya, J. Electrochem. Soc. **138**, 1018 (1991)
23. I. Riess, in *The CRC Handbook of Solid State Electrochemistry*, ed. by P.J. Gellings, H.J.M. Bouwmeester (Boca Raton, CRC, 1997), pp. 223–268
24. S. Carter, A. Selcuk, J. Chater, R.J. Kajda, J.A. Kilner, B.C.H. Steele, Solid State Ionics **53–56**, 597 (1992)
25. R. Koc, H.U. Anderson, J. Mater. Sci. **27**, 5477 (1992)
26. M. Oishi, K. Yashiro, K. Sato, J. Mizusaki, T. Kawada, J. Solid State Chem. **181**, 3177 (2008)
27. J. Cihlar, D. Del Favero, J. Cihlar Jr., A. Buchal, J. Van herle, J. Eur. Ceram. Soc. **26**, 2999 (2006)
28. T. C. Mazanec, The ECS Proceedings Series (Ceramic Membranes 1), ed by H. U. Anderson, et al., Pennington, NJ, **PV95-24**, 16 (1997)
29. S. Wang, "Oxygen Transport in Mixed Conducting Perovskite Oxides," Thesis, University of Houston, Houston, USA (2000)
30. J. Yoo, A. Verma, and A. J. Jacobson, The ECS Proceedings Series (Ionic and Mixed Conducting Ceramics IV), ed. by T. A. Ramanarayanan, et al., Pennington, NJ, **PV 2001-28**, 27 (2002)
31. J. Yoo, C. Park, A.J. Jacobson, Solid State Ionics **175**, 55 (2004)
32. J. Yoo, A.J. Jacobson, J. Electrochem. Soc. **156**(9), B1085 (2009)
33. J.S. Anderson, Proc. R. Soc., A **185**, 69 (1946)
34. P. Hagenmuller, M. Pouchard, J.C. Grenier, Solid State Ionics **43**, 7 (1990)
35. C. Park, A.J. Jacobson, J. Electrochem. Soc. **152**(7), J65 (2005)
36. L.M. Liu, T.H. Lee, L. Qiu, Y.L. Yang, A.J. Jacobson, Mater. Res. Bull. **31**(1), 29 (1996)
37. V.L. Kozhevnikov, I.A. Leonidov, M.V. Patrakeev, E.B. Mitberg, J. Solid State Chem. **158**, 320 (2000)
38. H. L. Tuller, in "*Nonstoichiometric Oxides*," ed. by O. Toft Sørensen (Academic press, New York 1981), pp 271–335
39. B.K. Flandermeyer, M.M. Nasrallah, A.K. Agarwal, H.U. Anderson, J. Am. Ceram. Soc. **67**(3), 195 (1984)
40. C. Wagner, Prog. Solid State Chem. **6**, 1 (1971)
41. J. Mizusaki, M. Yoshihiro, S. Yamauchi, K. Fueki, J. Solid State Chem. **58**, 257 (1985)